EUMETSAT Satellite Application Facility on Climate Monitoring

Algorithm Theoretical Basis Document

Cloud Physical Products

AVHRR / SEVIRI

Reference Number: SAF/CM/KNMI/ATBD/CPP

Issue/Revision Index: 1.0

Date: 12.02.2010

Document Signature Table

	Name	Function	Signature	Date
Author	Jan Fokke Meirink Rob Roebeling Erwin Wolters Hartwig Deneke	CM-SAF scientists		28/01/2010
Editor	Jörg Schulz	Science Coordinator		12/02/2010
Approval	Jörg Schulz	Science Coordinator		16/02/2010
Release	Martin Werscheck	SAF Manager		15/02/2010
Eumetsat Approval	Lothar Schüller	SAF Coordinator		

Distribution List

Internal Distribution	
Name	**No. Copies**
DWD Archive	1
CM-SAF Team	1

External Distribution		
Company	**Name**	**No. Copies**
PUBLIC		

Document Change Record

Issue/ Revision	Date	DCN No.	Changed Pages/Paragraphs
1.0	15/02/2010	SAF/CM/KNMI/ATBD/CPP	Initial release

Table of Contents

List of figures

List of tables

1. Introduction

This CM-SAF Algorithm Theoretical Basis Document (ATBD) provides detailed information on the retrieval algorithm deriving cloud physical products (CPP) from VIS-NIR-IR satellite imagers. Currently, this algorithm is used in the CM-SAF to derive daily and monthly mean cloud optical thickness (COT), cloud thermodynamic phase (CPH) and cloud liquid water path (LWP) from the geostationary MSG-SEVIRI and the polar-orbiting NOAA and METOP AVHRR instruments. The corresponding product numbers are CM-32/CM-33 for COT, CM-36/CM-37 for CPH, and CM-41/CM-42 for LWP. Details about these cloud physical products can be found in the product user manual (AD-1). The quality of the products is discussed in the validation reports AD-2, AD-3, and AD-4. In these validation reports, the product accuracy is evaluated against the Service Specifications (AD-5), while the product requirements are reported in AD-6. Further validation results are presented in Roebeling et al. (2008) and Wolters et al. (2008). The algorithm description in this document is largely based on Roebeling (2008).

Apart from the VIS-NIR-IR cloud physical products, a cloud thermodynamic phase product (CPH-IR) is retrieved solely from IR observations. The CPH-IR algorithm outlined in this ATBD is identical to the MODIS algorithm (Menzel et al. 2002).

The cloud physical properties retrieval algorithms are run for cloudy pixels only. The selection of cloudy pixels is done on the basis of the NWC-SAF cloud mask, also used in the CM-SAF for the determination of cloud fraction (AD-7 and AD-8).

In Section 2 an overview of the retrieval algorithms is presented. Section 3 gives a detailed description of the retrieval algorithms, consisting of the relevant underlying physics (Section 3.1), the radiative transfer modelling (Section 3.2), the implementation of the retrieval scheme (Section 3.3), the error budget of the retrieved products (Section 3.4), and the practical application of the algorithms (Section 3.4.2). Finally, assumptions and limitations are discussed in Section 4. Most sections consist of two parts, for the VIS-NIR-IR cloud physical properties and the IR cloud phase, respectively.

1.1. Applicable documents

Reference	Title	Code
AD-1	Product User Manual CLOUDS	SAF/CM/DWD/PUM/CLOUDS/1.2
AD-2	Annual Validation Report 2008	SAF/CM/DWD/VAL/OR4/1.1
AD-3	Annual Validation Report 2007	SAF/CM/DWD/VAL/OR3/2.0
AD-4	Scientific Report: Validation of CM_SAF cloud products derived from MSG/SEVIRI data	SAF/CM/DWD/KNMI/SMHI/SR/CLOUDS-ORR/3
AD-5	CDOP Service Specifications	SAF/CM/DWD/SeSp/1.6
AD-6	CDOP Product Requirements Document	SAF/CM/DWD/PRD/1.5
AD-7	Algorithm Theoretical Basis Document CM-SAF Product CM-03 and CM-04 Cloud Fraction from AVHRR	SAF/CM/SMHI/ATBD/CFC_AVHRR/1.0

Reference	Title	Code
AD-8	Algorithm Theoretical Basis Document CM-SAF Product CM-02, CM-08 and CM-14 Cloud Fraction, Cloud Type and Cloud Top Parameter Retrieval from SEVIRI	SAF/CM/DWD/ATBD/CFC_CTH_CTO_SEVIRI/1.0

2. Algorithm Overview

The CPP (cloud physical properties) algorithm, developed at KNMI, retrieves cloud optical thickness at visible wavelengths (COT or τ), cloud particle effective radius (r_e), cloud thermodynamic phase (CPH), and liquid/ice/total cloud water path (LWP/IWP/CWP). Presently, daily and monthly mean COT, CPH and CWP are produced as official CM-SAF products, both for geostationary (MSG-SEVIRI) and polar-orbiting (NOAA/METOP-AVHRR) imagers. The retrieval scheme was first described in Roebeling et al. (2006), and is based on earlier methods that retrieve cloud optical thickness and cloud particle size from satellite radiances at wavelengths in the non-absorbing visible and the moderately absorbing solar infrared part of the spectrum (Nakajima and King 1990; Han et al. 1994; Nakajima and Nakajima 1995; Watts et al. 1998). Since backscattered solar radiation is used, the algorithm is only applicable during daylight. Therefore, a separate retrieval scheme for cloud thermodynamic phase (CPH-IR), based on emitted thermal radiation and thus applicable during day and night, is used in addition. The CPH-IR algorithm is identical to the MODIS algorithm, outlined in Menzel et al. (2002). Further background on the retrieval principles can be found in Ackerman et al. (1990), Strabala et al. (1994), and Baum et al. (2000).

3. Algorithm description

3.1. Theoretical description

3.1.1. VIS-NIR-IR cloud physical properties

The principle of the CPP retrieval algorithm is that the reflectance of clouds at a non-absorbing wavelength in the visible region (VIS: 0.6 or 0.8 μm) is strongly related to the optical thickness and has little dependence on particle size, whereas the reflectance of clouds at an absorbing wavelength in the near-infrared region (NIR: 1.6 or 3.9 μm) is primarily related to particle effective radius. Moreover, Figure 1 shows that the imaginary parts of the refractive indices of water and ice, which are a measure for absorption, differ. For example, around 1.6 μm ice particles are more absorbing than water droplets. This feature, together with the use of an infrared (IR) window channel to inform on cloud-top temperature, allows to retrieve cloud thermodynamic phase. Liquid Water Path (LWP) can be computed from the retrieved τ and r_e by (Stephens 1978):

$$LWP = \frac{2}{3}\tau r_e \rho_l \qquad (1)$$

where ρ_l is the density of liquid water. Ice Water Path (IWP) is retrieved with the same formula using the effective radii of ice crystals.

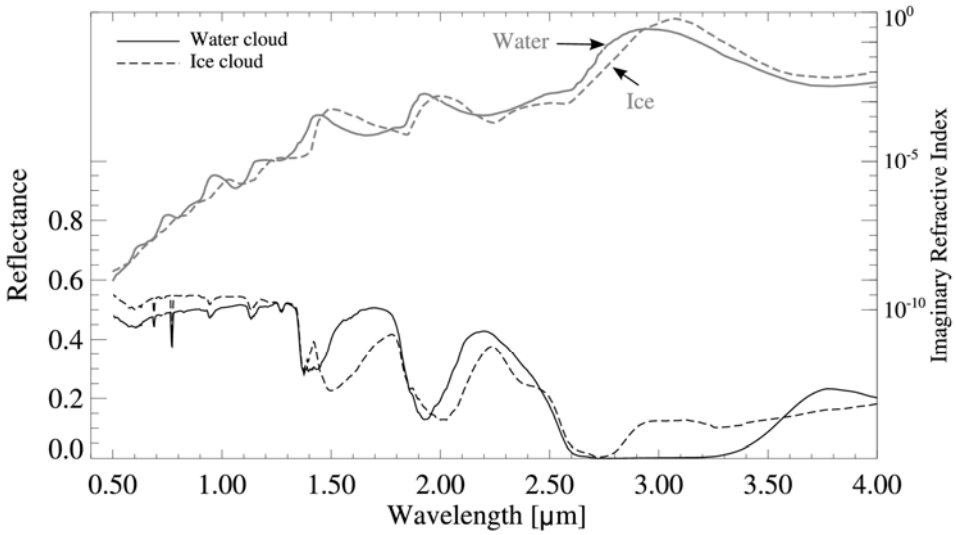

Figure 1: Simulated TOA reflectance spectra for a stratocumulus (water) cloud and a cirrus (ice) cloud, and the imaginary part of the index of refraction of water and ice. The simulations were made with MODTRAN at θ_0 = 45°, θ = 0° and φ = 0°. The reflectances are plotted as black lines, while the refractive indices are plotted as gray lines.

3.1.2. IR cloud phase

The MODIS bispectral infrared cloud phase algorithm is part of the MODIS Atmosphere Science Dataset (SDS), which is currently in its fifth reprocessing cycle (Collection 5, see for more information http://modis.gsfc.nasa.gov/). It uses the combination of 8.5-11 μm brightness temperature difference (hereafter referenced as $\Delta T_{8.5\text{-}11}$) and 11-μm brightness temperature, T_{11}, to determine cloud phase (Menzel et al., 2002; Platnick et al. 2003). It originally existed as a trispectral algorithm using $\Delta T_{8.5\text{-}11}$ and $\Delta T_{11\text{-}12}$ (Strabala et al. 1994, Ackerman et al. 1990). The method relies on the fact the imaginary parts of the index of refraction for water and ice particles are nearly equal between 8 and 10 μm but diverge between 10 and 13 μm, ice absorbing more radiation in the latter wavelength range (Figure 2). As a result, all else being equal, an ice cloud tends to have greater values of $\Delta T_{8.5\text{-}11}$ than a water cloud. Additionally, T_{11} itself gives an indication of the cloud top temperature and the probably corresponding thermodynamic phase.

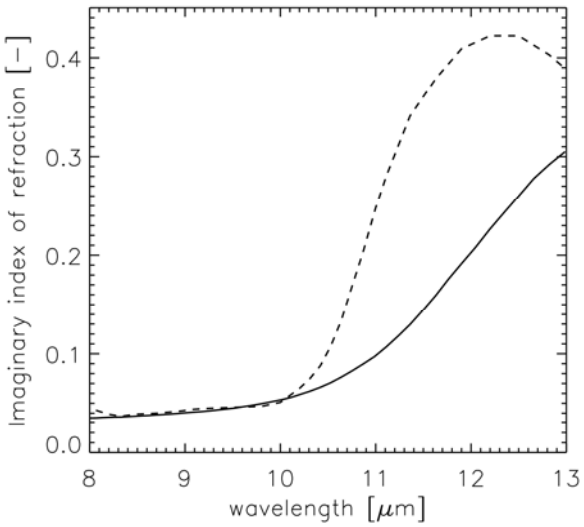

Figure 2: Imaginary index of refraction for water (solid line) and ice particles (dashed line) for the 8-13 μm spectral region (from Wolters et al, 2008). Water indices are from Downing and Williams (1975); ice indices are from Warren (1984).

3.2. Radiative transfer

The CPP algorithm compares satellite observed reflectances at visible and near-infrared wavelengths to look-up tables (LUTs) of simulated reflectances for given cloud optical thicknesses, particle sizes and surface albedos for water and ice clouds (Watts et al. 1998; Jolivet and Feijt 2003). The Doubling Adding KNMI (DAK) radiative transfer model has been used to generate the LUTs of simulated cloud reflectances. DAK has been developed for line-by-line or monochromatic multiple scattering calculations at UV, visible and near infrared wavelengths in a horizontally homogeneous cloudy atmosphere using the doubling-adding method (De Haan et al. 1987; Stammes 2001). The clouds are assumed to be plane-parallel and embedded in a multi-layered Rayleigh scattering atmosphere. The particles of water clouds are assumed to be spherical droplets with effective radii between 1 and 24 μm and an effective variance of 0.15. For ice clouds homogeneous distributions of imperfect hexagonal ice crystals (Hess et al. 1998) are assumed with effective radii between 6 and 51 μm. Knap et al. (2005) demonstrated that these crystals give adequate simulations of total and polarized reflectances of ice clouds.

Figure 3 shows an example of DAK calculations of 0.6 and 1.6 μm reflectances as function of τ and r_e for water droplets and ice crystals. The figure illustrates that for optically thick clouds ($\tau > 16$) lines of equal τ and particle size are nearly orthogonal, meaning that the 0.6 and 1.6 μm reflectances contain independent information on τ and r_e, respectively. This is not the case for optically thin clouds. Moreover, for these clouds, the lines of different r_e are very close together, implying that the retrieval of particle size is inherently uncertain. Finally, comparing the two panels in Figure 3, it is evident that ice clouds have a lower 1.6-μm reflectance than water clouds, which is a consequence of the stronger absorption of ice particles compared to water droplets at the 1.6 μm wavelength (Knap et al. 1999; Jolivet and Feijt 2003).

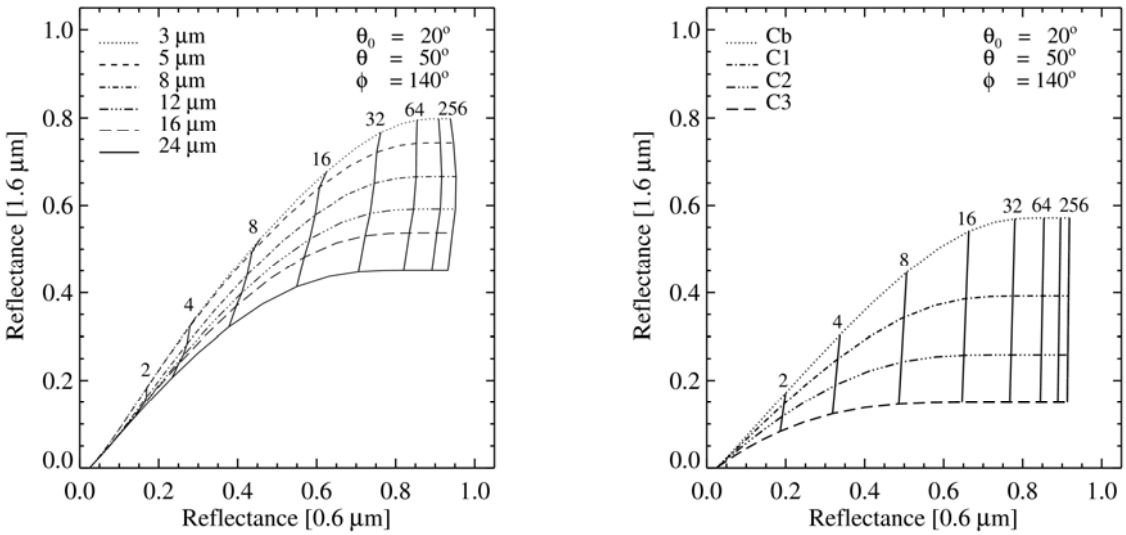

Figure 3: DAK calculations of TOA reflectance at 0.6 µm versus 1.6 µm for clouds consisting of spherical droplets with effective radii between 3 and 24 µm (left panel) and imperfect hexagonal columns Cb, C1, C2 and C3 (right panel). The reflectances have been calculated over a black surface (albedo = 0). Solar and satellite angles are indicated in the plots. The vertically oriented lines represent lines of equal cloud optical thicknesses between 0 and 256, while the horizontally oriented lines represent lines of equal particle size**.**

Table 1: Properties of the cloudy atmosphere and the surface that are used for the radiative transfer calculations to generate the LUTs.

Parameter	***Settings***				
Vertical profiles of pressure, temperature, and ozone	Midlatitude summer [a]				
Aerosol model	None				
Cloud height	1000 - 2000 m				
Solar zenith angle (θ_0) [b]	0 - 78.7° (≈equidistant in cos(θ_0), 65 points)				
Viewing zenith angle (θ) [b]	Same as θ_0				
Relative azimuth angle (ϕ) [b]	0 - 180° (equidistant, 91 points)				
Cloud optical thickness	0 – 256 (equidistant in log(τ), 22 points)				
	water clouds	**ice clouds**			
Cloud particle type	Spherical water droplet	Imperfect hexagonal ice crystal [c]			
Cloud particle size	1 –24 µm (1, 3, 5, 8, 12, 16, 24 µm)	Type	*D* (µm)	*L* (µm)	r_e (µm)
		Cb	4.0	10.0	6.0
		C1	10.0	30.0	12.0
		C2	22.0	60.0	26.0
		C3	41.0	130.0	51.0
Size distribution	Two-parameter gamma			-	
Effective variance (v_e)	0.15			-	

[a] The midlatitude summer atmosphere model was taken from Anderson et al. (1986).

[b] The chosen distributions of angles are motivated in Wolters et al. (2006).

[c] The imperfect hexagonal crystals are obtained from Hess et al. (1998) and have a distortion angle of 30°. The crystals are characterized by their length (*L*), diameter (*D*) and volume equivalent effective radius (r_e).

summarizes the governing characteristics of the cloudy atmosphere, together with information about intervals of cloud properties and viewing geometries used in the DAK simulations to generate the LUT. The DAK simulations were done for a black surface. The TOA reflectance $R(\alpha_s)$ over a surface with reflectance α_s is computed using (Chandrasekhar, 1960):

$$R(\alpha_S) = R_0 + \frac{\alpha_s t(\theta_0) t(\theta)}{1 - \alpha_s \alpha_a} \quad (2)$$

Here, $t(\theta_0)$ and $t(\theta)$ are the atmospheric transmission at the solar and viewing zenith angles, respectively, R_0 is the atmospheric reflectance above a black surface, and α_a the hemispherical sky albedo for upwelling, isotropic radiation. The required parameters are determined from two additional DAK calculations with surface reflectance values of 0.5 and 1.0.

3.3. Retrieval scheme

3.3.1. VIS-NIR-IR cloud physical properties

The cloud optical thickness and particle size are retrieved for cloudy pixels in an iterative manner as illustrated in Figure 4. During the iteration the retrieval of τ at the 0.6-μm channel is used to update the retrieval of r_e at the 1.6-μm channel. This iteration process continues until the retrieved cloud physical properties converge to stable values. The interpolation between cloud physical properties in the LUTs is done with polynomial interpolation for τ and linear interpolation for r_e. As stated above, the retrieved particle size values are unreliable for optically thin clouds. Therefore, for clouds with τ <8 assumed climatologically averaged effective radii of 8 μm and 26 μm for water and ice clouds, respectively, are used, close to the values used by Rossow and Schiffer (1999). To obtain a smooth transition between assumed and retrieved r_e a weighting function is applied for clouds with 0< τ <8.

The cloud thermodynamic phase (CPH) is determined as follows. The iterative process described above is first applied using the ice cloud LUT. If convergence is achieved and the cloud-top temperature (T_c) is lower than 265 K, the phase 'ice' is assigned. If not, the phase 'water' is assigned, and the iterative process to find τ and r_e is applied using the water cloud LUT.

The cloud top temperature is calculated from the 11-μm brightness temperature and the cloud emissivity. For optically thin clouds the observed brightness temperature represents the upwelling radiance at cloud top I_λ, which is determined by contributions from both the cloud and the surface below and can be approximated by:

$$I_\lambda = \varepsilon_\lambda B_\lambda(T_c) + (1 - \varepsilon_\lambda) B_\lambda(T_s) \quad (3)$$

where $B_\lambda(T)$ denotes the Planck function at temperature T and wavelength λ, ε_λ the emissivity of the cloud at wavelength λ, T_c the cloud top temperature and T_s the surface temperature. The emissivity is defined as the ratio of the radiance emitted by a cloud to the radiance emitting by a body that would obey the Planck function. In the absence of scattering the cloud emissivity can be approximated as a function of the absorption optical thickness at

wavelength λ (τ_λ) and the cosine of the satellite zenith angle (θ) as follows (Minnis et al. 1993):

$$\varepsilon_\lambda = 1 - \exp\left(\frac{-\tau_\lambda}{\cos\theta}\right). \qquad (4)$$

The (absorption) cloud optical thickness in the infrared (τ_{tir}) is related to the (scattering) cloud optical thickness in the visible (τ_{vis}). This relationship depends on particle size and thermodynamic phase. For large water and ice particles $\tau_{tir} \approx 0.5\,\tau_{vis}$ (Minnis et al. 1993). With ε_λ known, T_c is calculated from Equation (2), assuming a temperature difference between the surface and the cloud top of 10 K.

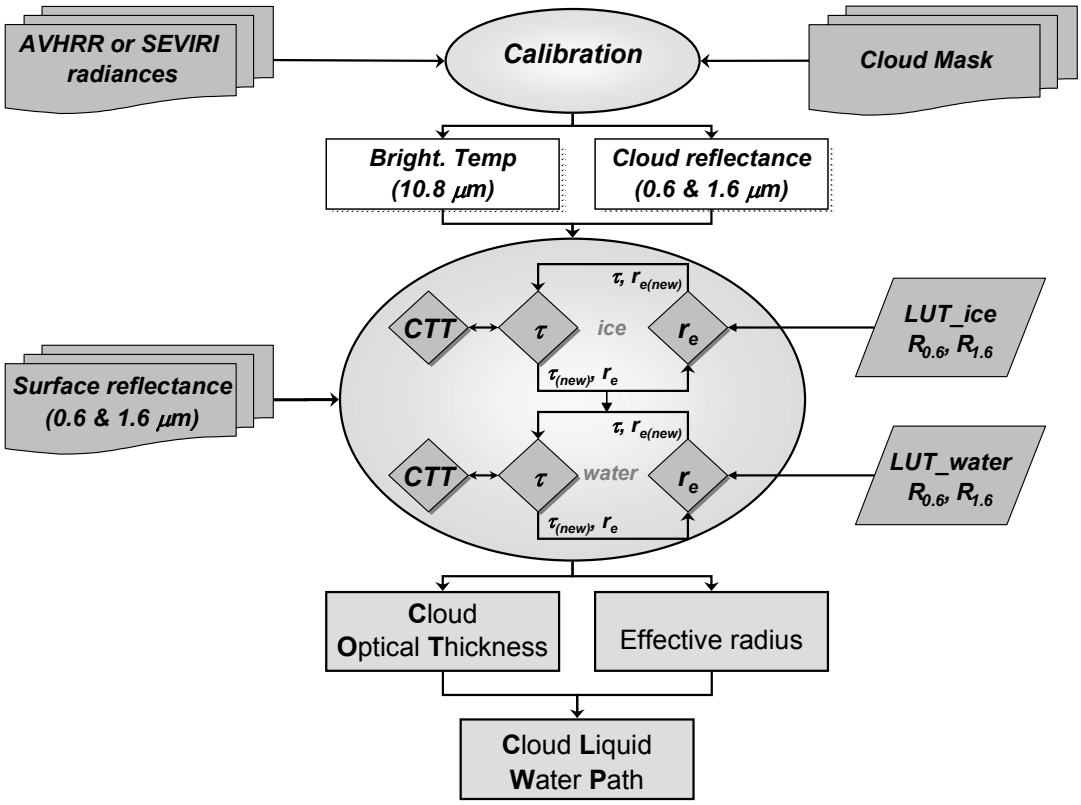

Figure 4: Flowchart of CPP algorithm for determining τ, r_e and LWP using look up tables of DAK-simulated 0.6- and 1.6-μm reflectances and cloud top temperatures derived from 10.8-μm brightness temperatures and τ.

3.3.2. IR cloud phase

The IR cloud phase algorithm uses the following thresholds for the respective thermodynamic phase categories:

- *water* (T_{11} > 238 K and $\Delta T_{8.5\text{-}11} \leq$ -1 K) or (T_{11} > 285 K and $\Delta T_{8.5\text{-}11} \leq$ -0.5 K);
- *ice* $T_{11} \leq$ 238 K and $\Delta T_{8.5\text{-}11} \geq$ 0.5 K;
- *mixed* 238 K < T_{11} < 268 K and -0.25 < $\Delta T_{8.5\text{-}11} \geq$ 0.5 K;
- *undetermined* all other $T_{11} - \Delta T_{8.5\text{-}11}$ combinations.

3.4. Error budget estimates

3.4.1. VIS-NIR-IR cloud physical properties

The retrieval of cloud optical thickness and effective radius from 2-channel backscattered solar radiation is a simple but heavily underconstrained problem. As a result, many uncertainties are associated to this retrieval problem (see Stephens and Kummerow (2007) for a review). Here we attempt to describe some of the most important error sources.

3.4.1.1. Errors in radiative transfer

To assess the potential error caused by uncertainties in radiative transfer modeling, Roebeling et al. (2005) compared four well-known RTMs that use different methods to solve the equation of radiative transfer. All these models are suited for simulating short-wave and narrow-band radiances in a cloudy atmosphere. However, the codes have originally been developed and optimized for different applications. The following methods for solving radiative transfer were compared:

- Monte Carlo method

The Monte Carlo model (Macke et al. 1999) is a forward scheme with a local estimate procedure for radiance calculations. It is a straightforward model that can be extended from one-dimensional to two- or three-dimensional calculations (Davis et al. 1985). Monte Carlo treats multiple scattering as a stochastic process. The phase function governs the probability of scattering in a specific direction. Photons are emitted by a source (e.g. the sun or a lidar device) and undergo scattering and absorption events inside a predefined three-dimensional cloudy atmosphere until: (i) the intensity of the photons falls below a certain threshold, (ii) the photons escape from the system, (iii) or the photons are absorbed by the atmosphere or the surface (forward scheme). After each scattering event, the intensity of the photons that contribute to predefined sensor viewing angles is calculated (local estimate procedure).

- Doubling Adding method

This is the method used in the DAK model introduced in Section 3.2. DAK first calculates the reflection and transmission of an optically thin layer, in which no more than two scattering events may occur. Thanks to this restriction the radiative transfer equation can be solved analytically. Next, the reflection and transmission of two identical layers on top of each other

can be obtained by computing successive reflections back and forth between the layers. This doubling procedure is continued until the actual optical thickness of the cloud is reached. The cloud is embedded in a multilayer Rayleigh scattering atmosphere. The DAK model includes polarization.

- Discrete Ordinates method

In the MODerate spectral resolution atmospheric TRANsmittance and radiance code (MODTRAN), the multiple scattering calculations are based on the Discrete Ordinate (DISORT) method (Stamnes et al. 1988). The radiative transfer equation is solved for *N* discrete zenith angles to obtain *N* equations for *N* unknowns. These unknowns may be solved numerically. The MODTRAN single scattering radiances are computed separately from DISORT with inclusion of spherical geometry effects; the plane-parallel DISORT single scattering contributions are subtracted from the DISORT radiances for generation of the total radiance values. For the comparisons a beta version, MODTRAN4v2r0, was used, in which user-defined phase functions for cloud particles could be specified.

- Spherical Harmonics method

The Spherical Harmonic Discrete Ordinate Method SHDOM (Evans 1998) has been developed for modeling radiative transfer in inhomogeneous three-dimensional media. SHDOM uses an iterative procedure to compute the source function of the radiative transfer equation on a grid of points in space. The angular part of the source function is represented by a spherical harmonics expansion mainly because the source function is computed more efficiently in this way than in DISORT. A discrete ordinate representation is used in the solution process. The number of iterations increases with increasing single scattering albedo and optical thickness.

The intercomparison study demonstrated that SHDOM and DAK are suitable models for the calculations of narrow-band cloud reflectances. For a clear atmosphere all models showed small absolute differences relative to the reference model (Monte Carlo), while for a cloudy atmosphere considerably larger absolute differences were observed. The causes for the latter differences are due to numerical noise or differences in the multiple scattering calculations. The implementation of a user defined phase function in MODTRAN4v2r0 (beta release) was a large improvement, it was still the least accurate model for the simulation of cloud reflectances in this study. On average MODTRAN simulations deviated less than 3% from the reference model, but for individual viewing angles in the principal plane the deviations can increase to about 30%. It was suggested that the differences in MODTRAN reflectances cannot be fully explained by the method for multiple scattering calculations (DISORT). Part of the observed differences may be explained by different or incorrect model parameterizations. However, MODTRAN has been further improved since the study by Roebeling et al. (2005). The DAK and SHDOM calculations were similar to Monte Carlo, with mean differences smaller than 3%. However, for individual cases the differences were occasionally much larger. A noticeable finding was that the Monte Carlo has a 3% bias as compared to SHDOM and DAK. This bias may be explained by differences in the treatment of the forward peak of the scattering phase function. Especially for large particles with a strong forward peak this may cause significant differences in simulated reflectances. Beside these differences, Monte Carlo showed small non-systematic oscillations relative to SHDOM and DAK. These oscillations were largest for optically thick clouds (τ = 64), for moderate particle sizes (r_e = 10 μm) and for large viewing zenith angles (75°). For these cases the number of multiple scattering events is large (up to 200) and the forward peak is strong, so that small differences in single scattering parameters can easily accumulate to large errors in

the reflectances (±2%). Finally, the used version of SHDOM became unstable at certain optical thicknesses and effective radii. Comprehensive analysis showed that these instabilities occur at 0.63 and 1.61 μm wavelengths and that the problem disappeared again by choosing another optical thickness or effective radius.

Errors in simulated reflectance translate non-linearly into errors in retrieved cloud properties, since the relationship between reflectance and cloud properties is non-linear. Figure 5 shows that, in particular, the cloud optical thickness retrieval becomes highly uncertain for thick clouds as a result of the asymptotic relation between visible reflectance R and cloud optical thickness τ. The derivative $d\tau/dR$ increases with increasing τ, and for large values of τ, a marginal change in visible reflectance causes a large increase in the retrieved cloud optical thickness. Figure 5 also shows that the error in retrieved τ grows towards large solar zenith angles. The effective radius (right panel) is less sensitive to errors in reflectance, and is generally less than 2 μm for thick clouds. However, for thin clouds (τ <4) the retrieval of r_e becomes highly uncertain (see discussion of Figure 3). Finally, large errors in cloud property retrievals can occur for particular vieiwing conditions, if a particular part of the phase function is sampled, e.g. the backward scattering peak or the cloudbow.

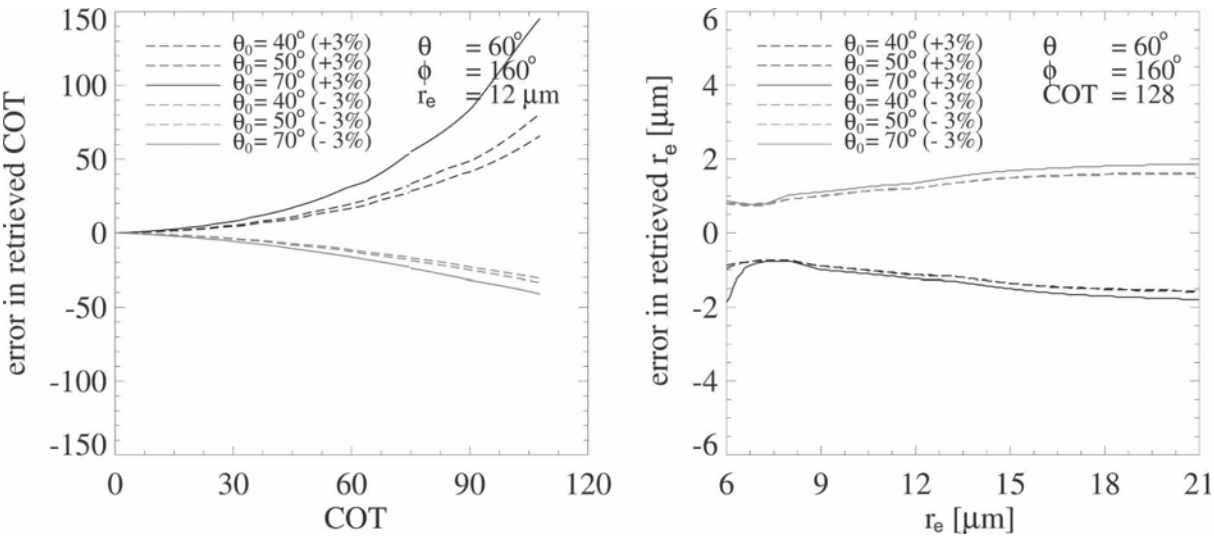

Figure 5: Error in retrieved (left) τ assuming errors of ±3% in the reflectance at 0.6 μm and (right) r_e assuming errors of ±3% in the reflectance at 1.6 μm. The errors have been calculated for θ_0 = 40°, 50°, and 70°, at θ = 60° and φ = 60°, and for r_e = 12 μm (left) and τ = 128 (right). From Roebeling et al. (2008).

3.4.1.2. Errors in ancillary data

Errors in geolocation, solar angles and satellite angles can be assumed to be small, and hence their impact on cloud property retrievals is limited. Larger errors can be caused by uncertainties in surface albedo. For thin or broken clouds over a bright (land) surface, a considerable part of TOA radiation comes from the surface. In these cases, an error in the surface albedo has consequences for the retrieved cloud properties. Finally, the cloud mask, which is external input to the CPP algorithm (and thus considered here as ancillary data), is of importance. The cloud mask determines for which satellite pixels a retrieval is performed.

It does not influence the retrieval itself, i.e. the level-2 products, but is does have impact on aggregated level-3 products. Typically, a more selective cloud mask (i.e. assigning less pixels cloudy) leads to a larger aggregated cloud optical thickness.

3.4.1.3. Instrument errors

The estimated reflectance calibration error of the AVHRR and SEVIRI instruments is 5% (see Table 2 and Table 3). However, in practice calibration errors can be much larger than that (e.g., Roebeling et al. 2006). The sensitivity calculations shown in Figure 5 demonstrate that this leads to large errors in retrieved cloud physical properties. Instrument (random) noise is probably smaller and thus much less of a problem.

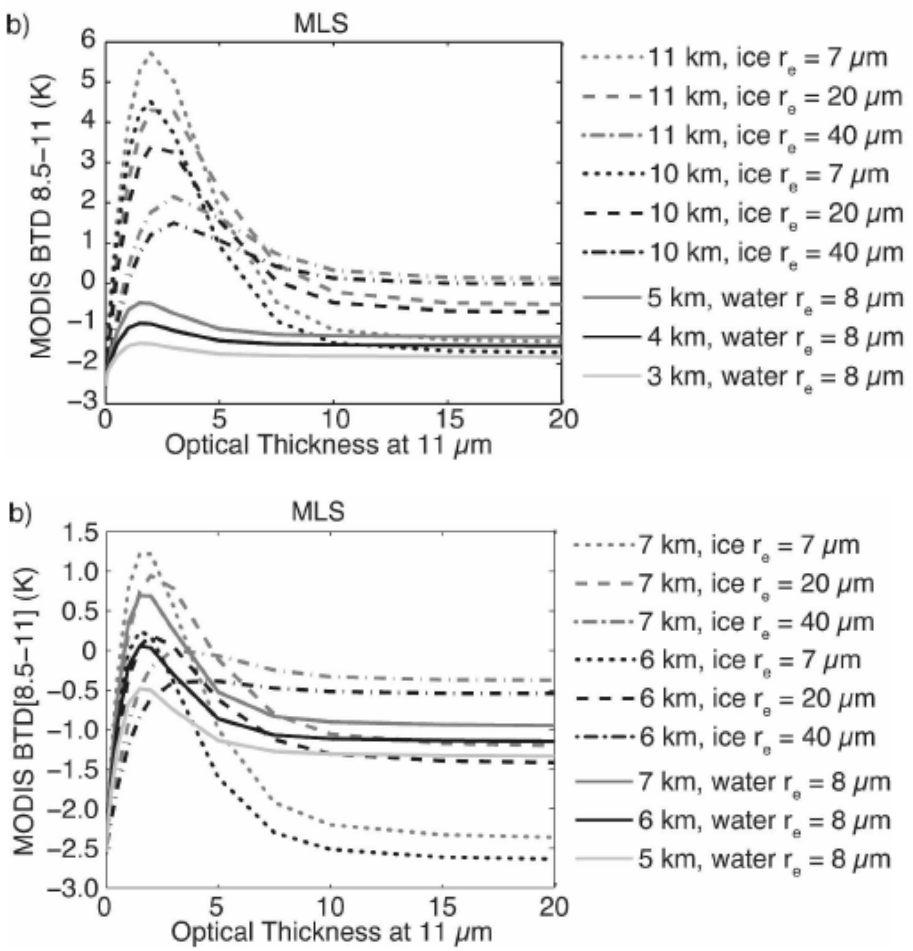

Figure 6: Simulated MODIS $\Delta T_{8.5\text{-}11}$ as a function of cloud optical thickness at 11 μm for ice and water clouds in a midlatitude summer atmosphere at (top) well-separated vertical levels and (bottom) levels with little vertical separation. (from Nasiri and Kahn, 2008).

3.4.2. IR cloud phase

Figure 6 presents simulated brightness temperature differences between 8.5 and 11 μm for ice and water clouds at various heights (Nasiri and Kahn, 2008). If there is sufficient vertical separation between ice and water clouds (top pannel), they can be reliably discerned from each other unless the IR optical thickness is very small or larger than ≈8 (corresponding to a

visible optical thickness of ≈16). For thicker clouds, the phase retrieval becomes ambiguous. However, for ice clouds with larger crystals unambiguous cloud-phase determination is still possible. The cloud-phase retrieval becomes problematic if water and and ice clouds have only little vertical separation (bottom panel). These conditions are particularly frequent in the storm tracks in both the Northern and Southern Hemispheres. The phase retrieval is also ambiguous when thin cirrus overlies a lower-level water cloud (i.e. multi-layered clouds).

Other error sources include:.

- errors due to non-uniform surface emissivities

The current version of the bispectral technique assumes a uniform surface emissivity for both IR bands. This is certainly not the case for many different ground surface types, including bare soils and deserts. Gao and Wiscombe (1994) modeled the effects of different surface types on the $\Delta T_{8.5\text{-}11}$ values based on laboratory surface emissivity measurements. Their results suggest that certain types of bare rock, and dry vegetation will lead to misidentification of cloud phase.

- calibration errors

The IR phase algorithm is sensitive to calibration errors, especially to errors in the relative calibration of the 8- and 11-μm channels, since the difference between the two is used. Instrument noise is also a potential source of error, but is not expected to be a major issue for SEVIRI.

3.5. Practical Application

The CPP retrieval algorithm is applied to the SEVIRI instruments on MSG as well as the AVHRR instruments on the NOAA and METOP satellites. Here we describe the characteristics of these instruments.

3.5.1. Satellite instruments

3.5.1.1. AVHRR

NOAA operates a series of polar orbiting satellites that carry the AVHRR instrument. Recently, EUMETSAT also launched an AVHRR instrument on the METOP polar orbiting satellite. The AVHRR passive imager operates six channels at wavelengths between 0.5 and 12.0 μm. Table 2 summarizes the spatial resolution, the spectral bands and the calibration accuracy for the visible, near-infrared and infrared channels on AVHRR. Due to fundamental constraints the data of only 5 channels are transmitted to the ground. The near-infrared 1.6 μm and 3.9 μm channels are time-shared. On NOAA-17 and METOP the 1.6-μm channel is operated during the daylight part of the orbit, while the 3.9-μm channel is operated during night. The other NOAA satellites currently transmit only data from the 3.9-μm channel. Since the CPP algorithm uses the VIS-0.6 and NIR-1.6 channels (in combination with TIR-10.8), the CPP products are currently only retrieved from NOAA-17 and METOP. The CPH-IR product is not retrieved from AVHRR.

Table 2: Spatial and spectral characteristics of AVHRR visible (VIS), near-infrared (NIR), and thermal infrared (TIR) channels.

Channel		*res. nadir (km)*	*Nominal spectral band (μm)*			*Calibration accuracy*
VIS	***0.6***	1	0.58	-	0.68	5%
VIS	***0.8***	1	0.73	-	1.00	5%
NIR	***1.6*** [a)]	1	1.58	-	1.64	5%
NIR	***3.9*** [a)]	1	3.55	-	3.93	0.12 K @ 300 K
TIR	***10.8***	1	10.30	-	11.30	0.12 K @ 300 K
TIR	***12.0***	1	11.50	-	12.50	0.12 K @ 300 K

[a)] Only one NIR channel at the same time can be transmitted to the ground.

3.5.1.2. SEVIRI

Meteosat Second Generation (MSG) is a series of European geostationary satellites that is operated by EUMETSAT. In August 2002 the first MSG satellite (METEOSAT-8) was launched successfully, while in December 2005 the second MSG satellite (METEOSAT-9) was launched. The MSG is a spinning stabilized satellite that is positioned at an altitude of about 36,000 km above the equator at 3.4° W for METEOSAT-8 and 0.0° for METEOSAT-9. The SEVIRI instrument scans the complete disk of the Earth 4 times per hour, and operates 12 channels simultaneously. An overview of the spatial and spectral characteristics of these channels is given in Table 3. Note that all six AVHRR channels have an analog with similar characteristics on SEVIRI. For the CPP algorithm the VIS-0.6 and NIR-1.6 channels are used in combination with the TIR-10.8, whereas the CPH-IR algorithm uses the TIR-8.7 and TIR-10.8 channels.

Table 3: Spatial and spectral characteristics of SEVIRI visible (VIS), near-infrared (NIR), thermal infrared (TIR), water vapor (WV), ozone (O_3), and carbon dioxide (CO_2) channels.

Channel		*res. nadir (km)*	*Nominal spectral band (μm)*			*Calibration accuracy*
HRVIS		1	0.40	-	1.10	5%
VIS	***0.6***	3	0.56	-	0.71	5%
VIS	***0.8***	3	0.74	-	0.88	5%
NIR	***1.6***	3	1.50	-	1.78	5%
NIR	***3.9***	3	3.48	-	4.36	0.35 K @ 300K
WV	***6.2***	3	5.35	-	7.15	0.75 K @ 250 K
WV	***7.3***	3	6.85	-	7.85	0.75 K @ 250 K
TIR	***8.7***	3	8.30	-	9.10	0.28 K @ 300 K
O_3	***9.7***	3	9.38	-	9.94	1.50 K @ 255 K
TIR	***10.8***	3	9.80	-	11.80	0.25 K @ 300 K
TIR	***12.0***	3	11.00	-	13.00	0.37 K @ 300 K
CO_2	***13.4***	3	12.40	-	14.40	1.80 K @ 270 K

3.5.2. Input data

In this section, the input data needed to run the CPP and CPH-IR algorithms are described. For the CPH-IR algorithm brightness temperatures for two channels (Section 3.5.2.1) and a cloud mask (Section 3.5.2.3) constitute the only required input.

3.5.2.1. Reflectances and brightness temperatures

The CPP algorithm needs reflectances from the 0.6- and 1.6-μm channels as well as brightness temperatures from the 10.8-μm channel. The CPH-IR algorithm needs brightness temperatures from the 8.7- and 10.8-μm channels.

3.5.2.2. Solar and satellite angles

The CPP algorithm requires the solar zenith angle θ_0, the satellite viewing zenith angle θ, and the relative sun-satellite azimuth angle ϕ. These angles are calculated by the NWC-SAF software and provided as input to CPP.

3.5.2.3. Cloud mask

A cloud mask is needed to decide for which pixels a cloud physical properties retrieval will be attempted. The cloud mask of the NWC-SAF is used for this purpose (see AD-7 and AD-8). The CPP and CPH-IR retrievals are run for pixels classified as *cloud contaminated* or *cloud filled*.

3.5.2.4. Surface albedo

Over land the surface albedo is prescribed from an average of three years of MODIS white-sky albedo data for the corresponding MODIS 0.6- and 1.6-μm channels. The white-sky albedo represents the bi-hemispherical reflectance in the absence of a direct component, which is a good estimate of the surface albedo below optically thick clouds (Moody et al. 2005). Over ocean the surface albedo is assumed to be 0.05 at both 0.6 μm and 1.6 μm.

4. Assumptions and Limitations

In this section some of the assumptions and limitations associated with the retrieval algorithms are listed. There are also general limitations related to the characteristics of the satellite instruments. Geostationary imagers have a limited spatial coverage compared to the global coverage provided by polar satellites. Additionally, geostationary imagers sample at a coarser resolution than polar imagers. For example, SEVIRI has a nominal resolution of 3x3 km^2 (but effectively only about 4.8x4.8 km), whereas for AVHRR this is 1x1 km^2. A coarser resolution gives rise to systematic biases in the derived cloud physical properties, as outlined in section 0. On the other hand, geostationary imagers resolve the diurnal cycle, with a temporal resolution of 15 minutes in the case of SEVIRI, whereas polar orbiters have only two overpasses per day in the tropics (of which one during nighttime) and up to ≈8 near the poles.

4.1. VIS-NIR-IR cloud physical properties

Specific limitations for the cloud physical products include:

- The derivation of cloud physical properties from reflected solar radiation is dependent on the availability of daylight. This means that no retrievals can be done during night time.
- Cloud retrievals are performed assuming that clouds are plane parallel. This is true only in a minority of cases, which implies that retrieval errors become larger as clouds deviate from being plane parallel. Especially convective clouds can be problematic, as they frequently have illuminated and shadowed sides (see, e.g., Marshak et al. 2006). Broken cloud fields can also cause problems for retrieving cloud properties, since a passive satellite sensor measures an averaged radiance of the cloudy and cloud-free part of a pixel. The error made in these cases is among others dependent on the contrast between clouds and underlying surface, the true properties of the cloud and the cloud fraction within the sampling resolution of the instrument (Oreopoulos and Davies 1998; Coakley et al. 2005; Wolters et al. 2010).
- The retrieval is highly problematic over very bright surfaces, particularly ice and snow, as the visible reflectance from clouds is similar to that from the surface.
- Unlike active satellite instruments, which can derive cloud profile information, retrievals from passive satellite instruments are limited by the fact that the obtained signal emanates from the integrated profile. Since near-infrared radiation is only penetrating into the cloud to a certain depth (due to absorption by cloud particles), the retrieved cloud phase and effective radius are representative for the upper part of the cloud (Platnick 2001). The penetration depth depends on the amount of absorption by cloud particles, which is increasing with wavelength. This means that the retrieved CPH and r_e depend on which NIR spectral channel is used (in our case 1.6-μm). See, for example, Rosenfeld et al. (2004) for a discussion on pro's and con's of the use of different NIR channels.
- In the derivation of Equation (1) for LWP it is assumed that the cloud particle effective radius does not vary with height. In reality this assumption is not satisfied. For example, liquid clouds often obey adiabatic theory leading to a slightly different relation for LWP, in which the factor 2/3 is replaced by 5/9. In general, the profile of r_e can have many different shapes.
- Many assumptions are made for the calculation of LUTs with DAK. These include: the absence of aerosols, the location of the cloud between 1 and 2 km height, the specific habits and resulting phase functions of ice crystals, and the type and width of water droplet effective radius distributions. The necessity of these assumptions is an illustration of the heavily underconstrained nature of the cloud physical properties retrieval principle.

4.2. IR cloud phase

The main assumptions and limitations of the CPH-IR algorithm have been described in Section 3.4.2. In short, the phase determination is problematic for (a) midlevel clouds, (b) very optically thin cirrus, (c) thick ice clouds with larger ice crystals, and (d) multi-layered clouds. A specific limitation is that the CPH-IR product cannot be derived from the AVHRR instrument, since it does not carry an 8.5-μm channel.

5. References

Ackerman, S.A., W.L. Smith, R.E. Revercomb, and J.D. Spinhirne, 1990: The 27–28 October 1986 FIRE IFO Cirrus Case Study: Spectral Properties of Cirrus Clouds in the 8–12 μm Window, *Mon. Wea. Rev.*, **118**, 2377-2388.

Anderson, G. P., S. A. Clough, F. X. Kneizys, J. H. Chetwynd, and E. P Shettle, 1986: AFGL Atmospheric Constituent Profiles (0-120km). Tech. Rep. AFGL-TR-86-0110, 43 pp.

Baum, B. A., P. F. Soulen, K. I. Strabala, M. D. King, S. A. Ackerman, W. P. Menzel, and P. Yang, 2000: Remote sensing of cloud properties using MODIS Airborne Simulator imagery during SUCCESS. II. Cloud thermodynamic phase. *J. Geophys. Res.*, **105**, 11,781-11,792.

Chandrasekhar S., 1960: *Radiative Transfer*, New York, Dover, 393 pp.

Coakley, J. A., M. A. Friedman, and W. R. Tahnk, 2005: Retrieval of cloud properties for partly cloudy imager pixels, *J. Atmos. Ocean. Technol.,* **22** , 3–17.

Davis, J. M., T. B. McKee, and S. K. Cox, 1985: Application of the Monte Carlo method to problems in visibility using a local estimate: an investigation. *Appl. Optics*, **24**, (19), 3193-3205.

De Haan, J. F., P. Bosma, and J. W. Hovenier, 1987: The adding method for multiple scattering calculations of polarized light, *Astron. Astrophys.*, **183**, 371-391.

Downing, H. D., and D. Williams, 1975: Optical constants of water in the infrared. *J. Geophys. Res.*, **80**, 1656–1661.

Evans, K. F., 1998: The Spherical Harmonics Discrete Ordinate, Method for Three-Dimensional Atmospheric Radiative Transfer. *J. Atmos. Sci.*, **55**, 429-446.

Gao, B.-C. and W. J. Wiscombe, 1994: Surface-induced brightness temperature variations and their effects on detecting thin cirrus clouds using IR emission channels in the 8-12 micron region. *J. Appl. Met.*, **33**, 568-570.

Han, Q., W. B. Rossow, and A. A. Lacis, 1994: Near-Global Survey of Effective Droplet Radii in Liquid Water Clouds Using ISCCP Data. *J. Climate,* **7**, 465-497.

Hess, H, R. B. A. Koelemeijer, and P. Stammes, 1998: Scattering matrices of imperfect hexagonal crystals. *J. Quant. Spectrosc. Radiat. Transfer*, **60**, 301–308.

Jolivet, D., and A. J. Feijt, 2003: Cloud thermodynamic phase and particle size estimation using the 0.67 and 1.6 micron channels from meteorological satellites. *Atm. Chem. and Phys.*, **3**, 4461-4488.

Knap, W. H., L. C. Labonnote, G. Brogniez, and P. Stammes, 2005: Modeling total and polarized reflectances of ice clouds: evaluation by means of POLDER and ATSR-2 measurements. *Appl. Optics*, **44**, 4060-4073.

Macke, A., D. Mitchell, and L. von Bremen, 1999: Monte Carlo radiative transfer calculations for inhomogeneous mixed phase clouds. *Phys. Chem. Earth*, **24-3**, 237-241.

Marshak, A., S. Platnick, T. Várnai, G. Wen, and R. F. Cahalan, 2006: Impact of three-dimensional radiative effects on satellite retrievals of cloud droplet sizes, *J. Geophys. Res.*, **111** , 9207–9218.

Menzel, W.P., B.A. Baum, K.I. Strabala, and R.A. Frey, 2002: Cloud top properties and cloud phase algorithm theoretical basis document, MODIS ATBD series, 62pp.

Minnis, P., K. N. Liou, and Y. Takano, 1993: Inference of Cirrus Cloud Properties Using Satellite-observed Visible and Infrared Radiances. Part I: Parameterization of Radiance Fields. *J. Atmos. Sci.*, **50**, 1279–1304.

Moody, E. G., M. D. King, S. Platnick, C. B. Schaaf, and F. Gao, 2005: Spatially complete global spectral surface albedos: Value-added datasets derived from Terra MODIS land products. *IEEE Transactions on Geoscience and Remote Sensing*, **43**, 144-158.

Nakajima, T., and M. D. King, 1990: Determination of the Optical Thickness and Effective Particle Radius of Clouds from Reflected Solar Radiation Measurements. Part 1: Theory. *J. Atmos. Sci* ., **47**, 1878-1893.

Nakajima, T. Y., and T. Nakajima, 1995: Determination of Cloud Microphysical Properties from NOAA AVHRR Measurements for FIRE and ASTEX regions. *J. Atmos. Sci.,* **52**, 4043 – 4059.

Nasiri, S.L., and B.H. Kahn, 2008: Limitations of Bispectral Infrared Cloud Phase Determination and Potential for Improvement, J. Appl. Meteor. Climatol., 47, 2895-2910, doi: 10.1175/2008JAMC1879.1.

Oreopoulos, L., and R. Davies, Plane parallel albedo biases from satellite observations. part I: Dependence on resolution and other factors, 1998: *J. Climate*, **11** , 919–932.

Platnick, S., 2001: A superposition technique for deriving mean photon scattering statistics in plane-parallel cloudy atmospheres, *J. Quant. Spectrosc. Radiat. Transfer*, **68**, 57-73

Platnick, S., King, M. D., Ackerman, S. A., Menzel, W. P., Baum, B. A., Riedi, J. C., Frey, R. A., 2003: The MODIS cloud products: Algorithms and examples from Terra. *IEEE Trans. Geosci. Remote Sens*., **41**, 459-473.

Roebeling, R. A., 2008: Cloud Physical Properties Retrieval for Climate Studies using SEVIRI and AVHRR data, PhD Thesis, Wageningen University, The Netherlands, 160pp. Available from http://www.knmi.nl/publications.

Roebeling, R. A., A. Berk, A. J. Feijt, W. Frerichs, D. Jolivet, A. Macke, and P. Stammes, 2005: Sensitivity of cloud property retrievals to differences in narrow band radiative transfer simulations, KNMI Scientific Report, WR 2005-02, Royal Netherlands Meteorological Institute, De Bilt, the Netherlands, 27 pp. Available from http://www.knmi.nl/publications.

Roebeling, R. A., A. J. Feijt, and P. Stammes, 2006: Cloud property retrievals for climate monitoring: implications of differences between SEVIRI on METEOSAT-8 and AVHRR on NOAA-17, *J. Geophys. Res.*, **111**, D20210, doi:10.1029/2005JD006990.

Roebeling, R.A., H. M. Deneke, and A. J. Feijt, 2008: Validation of cloud liquid water path retrieveals from SEVIRI using one year of CloudNET observations, *J. Appl. Meteorol. Clim*., **47**, 206-222.

Rosenfeld, D., E. Cattani, S. Melani, and V. Levizzani, 2004: Considerations on daylight operation of 1.6-versus 3.7-µm channel on NOAA and Metop satellites. *B. Am. Meteorol. Soc.*, **85**, 873–881.

Rossow, W.B., and R.A. Schiffer, 1999: Advances in understanding clouds from ISCCP. *B. Am. Meteorol. Soc*., **80**, 2261-2287.

Stammes, P., 2001: Spectral radiance modeling in the UV-Visible range. IRS 2000: Current problems in Atmospheric Radiation, edited by W.L. Smith and Y.M. Timofeyev, pp 385-388, A. Deepak Publ., Hampton, Va.

Stamnes, K., S. C Tsay, W. Wiscombe, and K Jayaweera, 1988: Numerically stable algorithm for discrete ordinate method radiative transfer in multiple scattering and emitting layered media. *Appl. Optics,* **27**, 2502-2509.

Stephens, G. L., 1978: Radiation profiles in extended water clouds: II. Parameterization schemes. *J. Atmos. Sci.*, **35**, 2123-2132.

Stephens, G. L. and C. D. Kummerow, 2007: The Remote Sensing of Clouds and Precipitation from Space: A Review. *J. Atmos. Sci*., **64** , 3742–3765.

Strabala, K. I., S. A. Ackerman and W. P. Menzel, 1994: Cloud properties inferred from 8-12 -µm data. *J. Appl. Meteorol.*, **33**, 212-229.

Warren, S. G., 1984: Optical constants of ice from the ultraviolet to the microwave. *Appl. Optics*, **23**, 1206–1225.

Watts, P. D., C. T. Mutlow, A. J. Baran, and A. M. Zavody, 1998: Study on Cloud Properties derived from Meteosat Second Generation Observations, Final Report, EUMETSAT ITT no. 97/181.

Wolters, E. L. A., H. M. Deneke, B. J. J. M. van den Hurk, J. F. Meirink, and R. A. Roebeling, 2010: Broken and inhomogeneous cloud impact on satellite cloud particle effective radius and cloud-phase retrievals, *J. Geophys. Res*., **115**, doi:10.1029/2009JD012205 (in press).

Wolters, E. L. A., R. A. Roebeling, and A. J. Feijt, 2008: Evaluation of cloud-phase retrieval methods for SEVIRI onboard Meteosat-8 using ground-based lidar and cloud radar data, *J. Appl. Meteorol. Clim.*, **47**, 1723-1738.

Wolters, E. L. A., R. A. Roebeling, and P. Stammes, 2006: Cloud reflectance calculations using DAK: study on required integration points, KNMI Technical Report, TR-292, Royal Netherlands Meteorological Institute, De Bilt, The Netherlands, 17 pp. Available from http://www.knmi.nl/publications.